REFLECTION

Research Article

Room Temperature Photoluminescence Studies on Mn Doped and Sr Co-doped CuO Nanostructures

Akhil M. Anand[1*], Jishad A. Salam[1] and Abraham. K. E[2]
[1]Department of Physics, University of Kerala, Karyavattom – 695581
[2]St. Berchmans College, Changanassery - 686101
[*]Corresponding authur (E-mail address: akhilmanand2@gmail.com)

Abstract

Nanoparticles of Copper Oxide (CuO), Manganese (Mn)-doped CuO, and Mn and Strontium (Sr) co-doped CuO were synthesised via co-precipitation method. The XRD results show that the particles were monoclinic in structure, and the crystallite size increased from 23.83 nm for CuO, 25.47 nm for CuO: Mn (0.1), 26.10 nm for CuO: Mn (0.2), 26.65 nm for CuO: Mn (0.3) and 28.31 nm for CuO: Mn (0.3): Sr co-doped samples. The band gap of the nanoparticles decreases in the same sequence from 2.97 eV for CuO to 2.40 eV for the co-doped samples. Morphological analyses were carried out using FESEM. The polygon shape of CuO particle changes to a stacked platelet-like structure with high porosity. Mn and Sr co-doped particles exhibit highly stacked platelet structures with less porosity, which showed a variation in sample morphology with doping. From EDS analysis, the Mn atomic percentage for CuO:Mn (0.1), CuO:Mn (0.2) and CuO:Mn(0.3) samples were found to be increased in accordance with the increase in doping concentration of Mn in the samples. Room temperature PL spectra obtained at excitation wavelengths 400 and 500 nm for CuO, CuO:Mn(0.1), CuO:Mn(0.2), CuO:Mn(0.3) and CuO:Mn(0.3):Sr samples show prominent defect level emissions.

1. Introduction

One of the most crucial arenas of current materials science and technology is the synthesis and characteristics of nanostructured materials. In addition to having potential uses in the development of electronic and optical nanodevices, nanomaterials represent a form of an ideal system for researching numerous physical aspects. The development of metal oxide nanomaterials is of great interest because metal oxides exhibit a wide variety of characteristics, ranging from wide band-gap insulators to metallic and superconducting. The synthesis and investigation of the physical and chemical properties of semiconducting oxides including ZnO, SnO_2, TiO_2, and In_2O_3 have received significant study attention [1]. One of the most significant semiconducting oxides is cupric oxide (CuO), which has a direct band gap of 1.85 eV and a monoclinic crystal structure. It may be used in high temperature superconductors, solar cells, catalysis, sensors, electrode materials, magnetic storage devices, lithium ion batteries, and electrode materials [2]. Doping semiconductor nanoparticles with metal ions is a potent way to change a material's physical properties. Several researchers have documented how different dopants have improved a material's distinguishing qualities [3]. Ahmed et al. discovered the

reduction of the band gap of Ni-doped SnO_2 nanoparticles, and Das et al. reported the tuning of the photoluminescence emission characteristics of manganese (Mn) doped Cu_2O nanoparticles. The least researched field is co-doping with strontium (Sr) and doping copper oxide with manganese. Thus, the current study's goal was to dope CuO with manganese and co-dope it with strontium while also examining the nanostructures' structural and optical characteristics [4,5].

2. Materials and methods
2.1 Synthesis of CuO nanoparticles

0.1 molar copper acetate $((CH_3COO)_2Cu.H_2O)$ (99.80% Merck) and sodium hydroxide (NaOH) (99.80% Merck) solutions were prepared in 100mL distilled water. The above-mentioned solutions were combined and stirred for an hour at room temperature using a magnetic stirrer. The resulting precipitate is centrifuged and repeatedly rinsed in distilled water. This precipitate was further annealed for 5 hours at 500 ^{0}C after being dried for 5 hours at 800 ^{0}C to produce the CuO nanoparticles. CuO nanoparticles were the finished black product that was produced.

2.2 Synthesis of Mn doped CuO nanoparticles

0.1 molar copper acetate $((CH_3COO)_2Cu.H_2O)$ and sodium hydroxide (NaOH) solutions were prepared separately in 100 ml distilled water. 0.002g manganese acetate (0.1 weight percentage of copper acetate) is dissolved in 100 ml distilled water. Cu acetate and Mn acetate solutions were mixed and stirred for 15 minutes. To the above mixture, sodium hydroxide solution is slowly added and continuously stirred for one hour. The precipitate was centrifuged and washed several times in distilled water. Then it was dried at 800°C for 5 hours, and then annealed at 500°C for 5 hours to get Mn-doped CuO nanoparticles. The same method was applied to prepare CuO:Mn(0.2) and CuO:Mn(0.3), two weight percentages of Mn doped CuO nanoparticles.

2.3 Synthesis of Mn:Sr doped CuO nanoparticles

This synthesis involves two steps. In the first step, Mn doped CuO nanoparticles were prepared as in the above method. Second step describes the doping of Sr in Mn doped CuO. 0.02 g strontium chloride ($SrCl_2$) (5 weight percentage of Mn doped CuO) is added to 0.4 g Mn doped CuO particles. This mixture is grinded continuously and uniformly for half an hour. The grinded mixture is annealed at 700 ^{0}C for 5 hours in high temperature tubular furnace under Ar atmosphere to obtain Mn:Sr doped CuO nanoparticles.

The morphological and material composition analysis of the samples was performed using a FE-SEM (Nova NANOSEM NPEP252, Equipped with X Slash detector 6/10 (Bruker) equipped with EDS (EDS-Quanpax 200, Germany) and a Bruker X-ray diffractometer with CuK radiation (λ=15.406 nm) in the 2 range from 0° to 90^0. A Xenon lamp was used as the excitation source for the PL observations in a luminescence spectrometer (Perkin Elmer LS-45) at room temperature. At room temperature, optical absorbance spectra in the wavelength

range of 200-900 nm were recorded using a T90 UV-Visible spectrophotometer, PG equipment.

3. Results and Discussions

3.1 Structural analysis
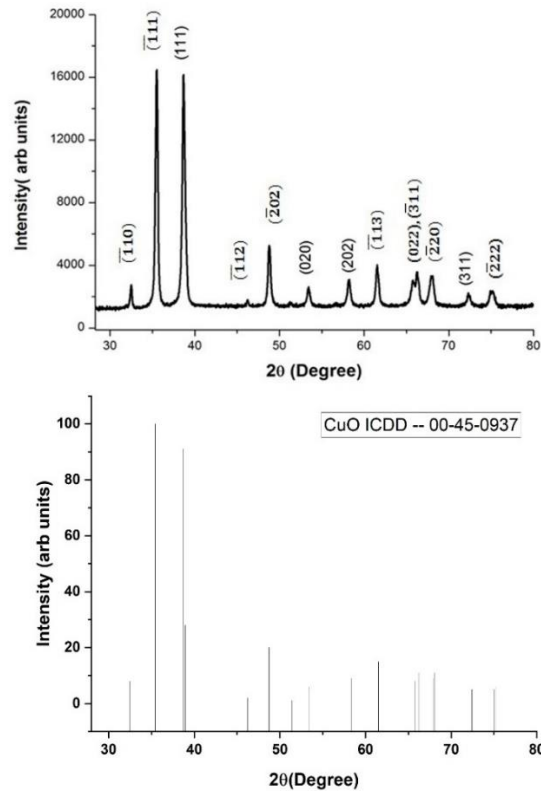
Figure.1: XRD Pattern of CuO nanoparticles

CuO's monoclinic structure can be seen in the sample's XRD peak positions (Figure 1), which was supported by the standard data (JCPDS file: 45-0937). Additionally, the XRD pattern showed no other impurity peaks, demonstrating the CuO sample's phase purity. Scherrer's formula revealed that the crystallite size was 23.83 nm. The lattice parameters of the monoclinic structure were found to be a= 4.685 Å, b= 3.425 Å, and, c= 5.130 Å and β= 99.549^0.
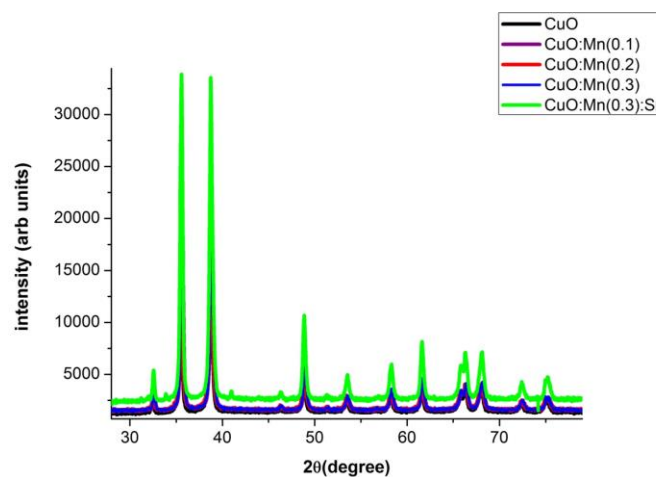
Figure 2: Variation of XRD intensity with doping

To investigate the impact of doping on CuO nanoparticles, CuO is first doped with manganese at various concentrations and then co-doped with strontium Peaks intensity of CuO nanostructure increases with the corresponding increment of Mn doping and Mn, Sr co-doping concentration to CuO, indicating the crystallinity improvement upon doping concentrations (Figure 2). Meanwhile, no changes have been observed in the peak positions over doping of Mn and Sr, which confirms the monoclinic structure of CuO remains unchanged after adding impurities. From XRD analysis, the crystallite size slightly increased to higher doping concentration and co-doping (Table 1).

Table 1: Variation of crystallite size with doping

Sample	Crystallite size (nm)
CuO	23.83
CuO:Mn (0.1)	25.47
CuO:Mn (0.2)	26.10
CuO:Mn (0.3)	26.65
CuO:Mn(0.3):Sr	28.31

In the case of Manganese (Mn) doped CuO, the XRD pattern does not contain any peaks of Mn atom. From which we can infer that Mn atom goes into the lattice of CuO in the form of Mn^{2+} ions replacing Cu^{2+} ions. The ionic radii of Mn^{+2} is 0.83 Å, which is greater than the ionic radius of Cu^{2+} (0.73 Å) [6]. Since Mn^{2+} has a greater ionic size than Cu^{2+}, Mn doping causes a modest increase in crystallite size. The particle size was found to be increased slightly with the increase in Mn concentration. When Mn (0.3) doped CuO is co-doped with strontium, as expected, crystalline size again increases. The ionic radius of Sr^{2+} is 1.18 Å, it is larger than ionic radius of $Cu^{2+.}$ Since ionic radius of Sr^{2+} is larger than $Cu^{2+,}$ crystallite size increases after Sr doping.

3.2 FE-SEM analysis

Powder samples were used for FESEM analysis. SEM micrographs images for CuO particles reveal the presence of polygons of various distinct shapes with dense continuous ordering. It is clearly seen that the sample morphology changes with doping. With Mn doping, the polygon shape of CuO particle changes to a stacked platelet like structures with less density, ordering and high porosity. Again, with Sr doping, CuO:Mn particles exhibit highly stacked platelet structures with less porosity. It shows more agglomeration than CuO:Mn samples.
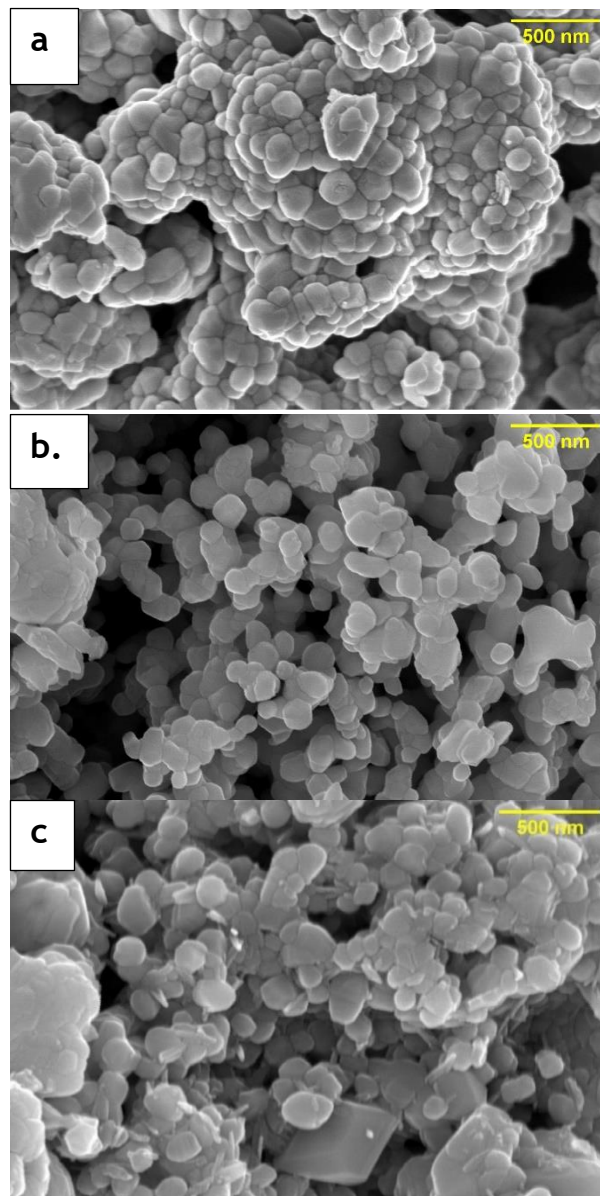
Figure 3: FE-SEM Image of (a). CuO nanoparticles, (b). CuO:Mn (0.3) nanoparticles, (c). CuO:Mn(0.3):Sr nanoparticles

3.3 Energy dispersive spectrum analysis

Energy dispersive spectrum (EDS) analysis is a technique used to determine the material composition (Figure 4). In doped samples presence of Mn and Sr were confirmed from the selected area EDS analysis. From EDS analysis, the Mn atomic percentage for CuO:Mn(0.1), CuO:Mn(0.2) and CuO:Mn(0.3) samples were found to be increased similar to the increase in doping concentration of Mn in the samples. The XRD and EDS data demonstrate that Mn and Sr have been successfully doped in CuO nanocrystals.
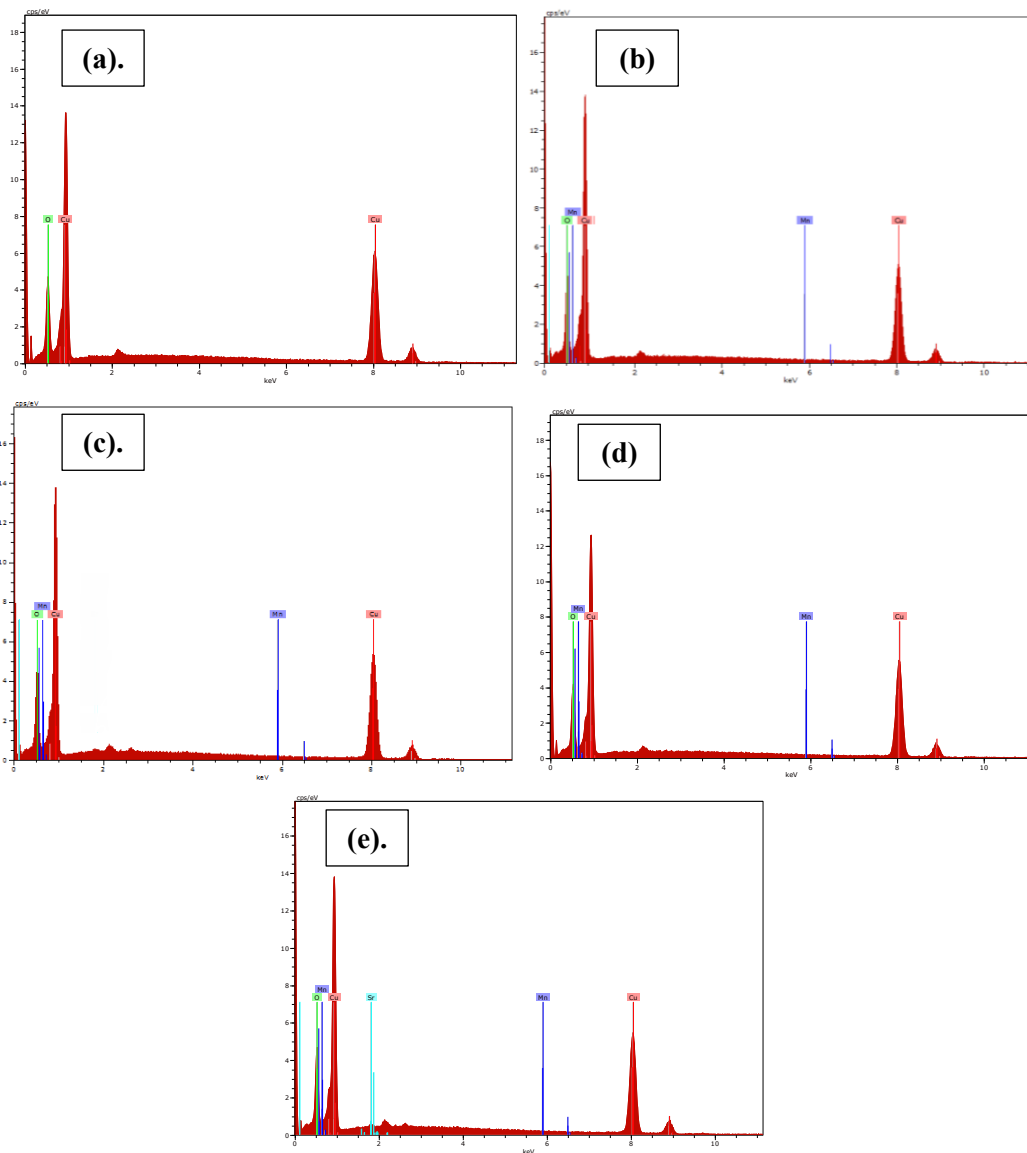
Figure 4: EDS Spectrum of (a). CuO nanoparticles, (b). CuO:Mn (0.1) nanoparticles, (c). CuO:Mn (0.2) nanoparticles, (d). CuO:Mn (0.3) nanoparticles, (e). CuO:Mn(0.3):Sr nanoparticles

3.4 UV-Visible Spectroscopy

The range of wavelengths that cover the energy between the valence band and conduction band extreme is one of the most crucial factors for optical applications of semiconducting materials because it provides the necessary knowledge about the region of transparency for the film material. The UV-visible absorption spectra of the nanoparticles CuO, CuO:Mn (0.1), CuO:Mn (0.2), CuO:Mn (0.3), and CuO:Mn(0.3):Sr are shown in Figure 5. Every sample has an absorption peak in the UV region.

The Tauc relation, which is shown below, is used to determine the magnitude of the direct band gap of CuO nanoparticles from the absorption spectra.

$$Ah\nu = A'(h\nu - E_g)^n$$
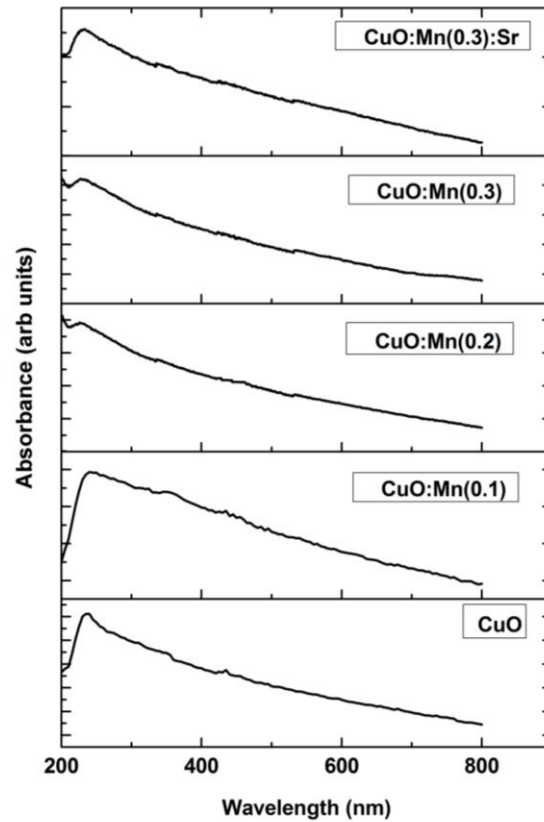
Figure 5: UV-Visible absorption spectra of CuO, CuO:Mn,CuO:Mn(0.3):Sr nanoparticles

The absorption coefficient is defined as = A/Cl, where A is the absorbance, l is the wave path length, which is equal to the cuvette's thickness, and C is the sample concentration. E_g is the band gap, hν is the photon energy, and n = 1/2 and 2 for direct and indirect band gap semiconductors, respectively, are the proportionality constant A′, Eg, and hν. Plotting $(αhν)^2$ versus photon energy (hν) provided the best linear relationship. By fitting a straight line to the linear component of the curve, the line fit to the $(αhν)^2$ against h plot is created. The value of the intercept of the straight line at = 0 was used to calculate the optical band gap. The Tauc plots of CuO, Mn doped CuO, and Mn:Sr doped CuO nanoparticles are displayed in Figure 6.
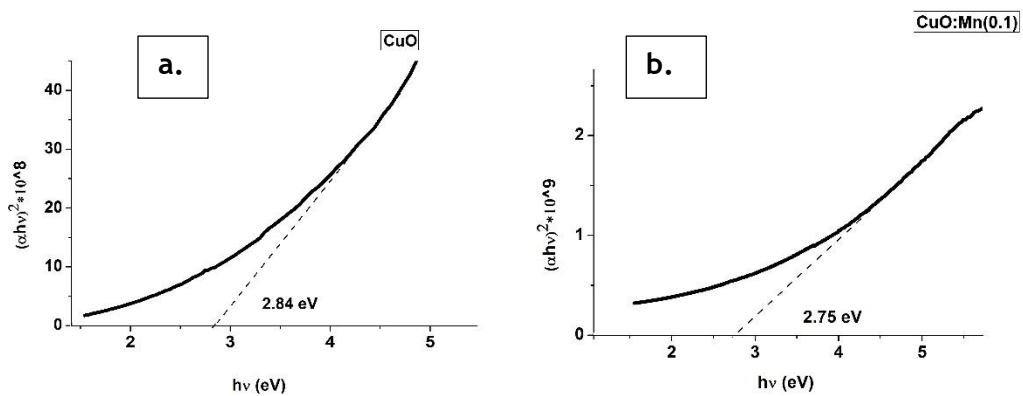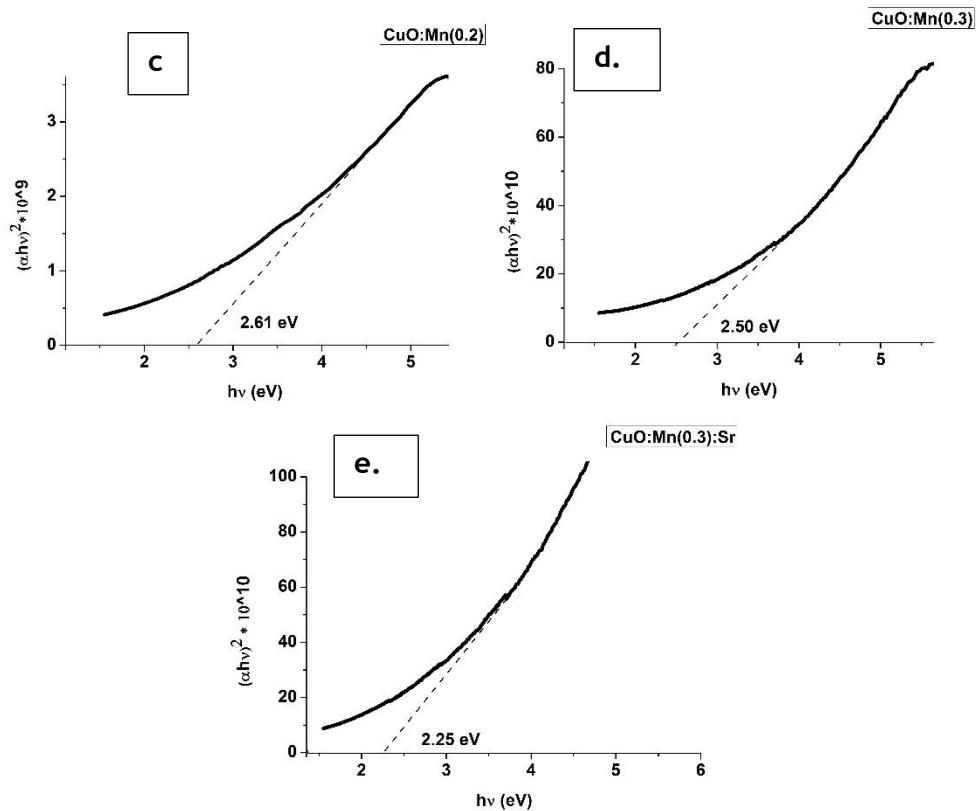
Figure 6: Tauc plots of CuO, CuO:Mn and CuO:Mn(0.3):Sr nanoparticles

The band gap of pure CuO nanoparticles is 2.84 eV, which is higher than the band gap of bulk CuO (1.85 eV), as can be observed from Tauc plots. This rise has been linked to the nanoparticles' quantum confinement effect [7]. CuO:Mn (0.1), CuO:Mn (0.2), and CuO:Mn (0.3) samples have optical band gaps of 2.75, 2.61, and 2.50 eV, respectively. The optical bandgap drops to 2.25 eV when strontium is co-doped with CuO:Mn (0.3) nanoparticles. According to the effective mass approximation, it is evident from Tauc plots that the band gap reduces with increasing dopant concentration and co-doping as a result of the growth in crystallite size [8].

$$\Delta E_g = \hbar^2\pi^2/2R^2\{1/m_e + 1/m_h\} - (1.786e^2)/\mathsf{J}\ R$$

Where m_h and m_e are the effective masses of holes in the valence band and electrons in the conduction band, respectively, and J is the material's static dielectric constant. Eg represents the widening of the semiconducting material's band gap. In the aforementioned equation, the particle-in-a-box quantum localization energy is represented by the first term, which has a straightforward $1/R^2$ dependence, and the Coulomb energy is represented by the second term, which also has a $1/R$ dependence. The value of ΔE_g will therefore drop when R rises as a result of the larger crystallites brought on by high temperature annealing.

3.5 Photoluminescence analysis

Room temperature photoluminescence spectrum of CuO (Figure 7), CuO:Mn (Figure 8) and CuO:Mn(0.3):Sr (Figure 9) are shown below. Emission spectra were taken using excitation wavelengths 400 and 500 nm for CuO, CuO:Mn and CuO:Mn(0.3):Sr samples respectively.
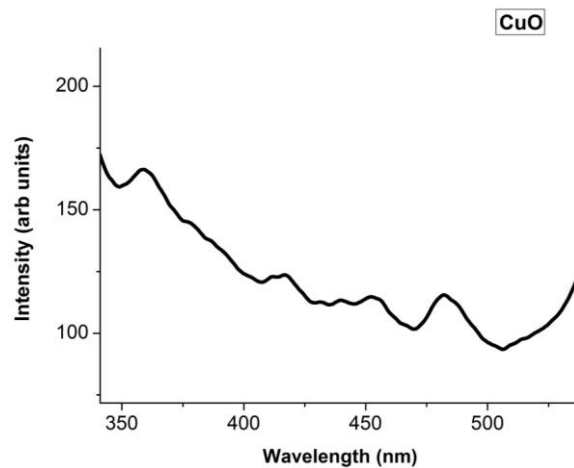
Figure 7: Photoluminescence spectrum of CuO nanoparticles
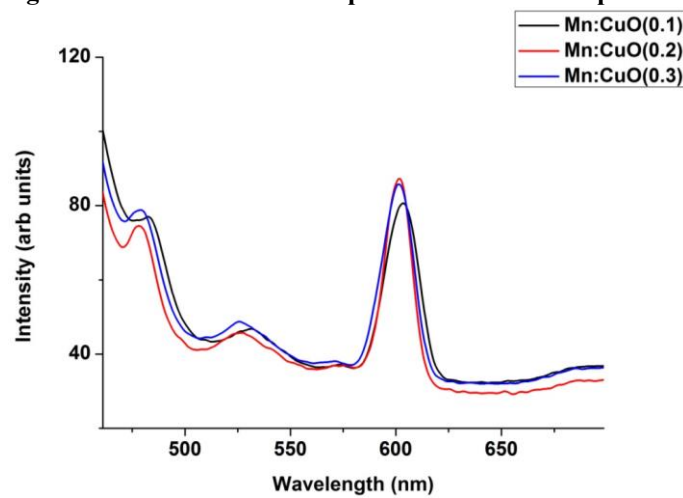
Figure 8: Photoluminescence spectrum of Mn:CuO nanoparticles
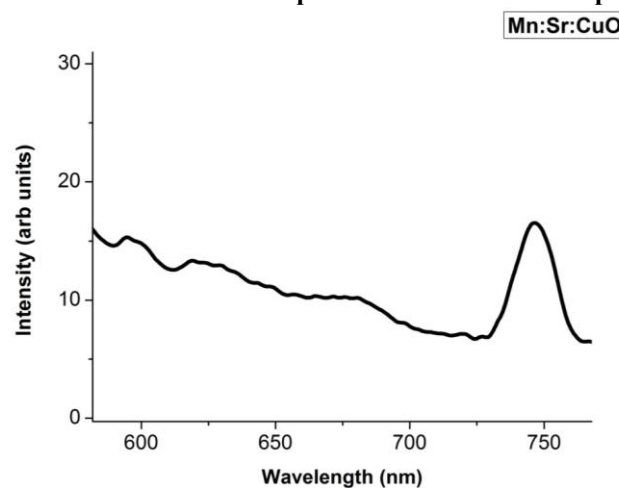
Figure 9: Photoluminescence spectrum of Mn:Sr:CuO nanoparticles

For CuO nanoparticles, the photoluminescence (PL) shows four peaks at wavelengths 417 (2.97 eV), 437 (2.84 eV), 450 (2.76 eV) and 483 (2.57 eV) nm. The peak at 437 nm can be attributed to the band gap emission of the CuO nano particles which was also confirmed from the UV-Vis analysis discussed in the previous section. The near band edge emission (NBE), which has a peak at 417 nm, is caused by the radiative recombination of an electron in the conduction band and a hole in the valence band [9]. Furthermore, oxygen vacancies and

inherent flaws are typically blame for the presence of higher wavelength emissions in oxide nanomaterials. It is widely known that the oxygen vacancies and interstitial metal ions in the oxide are responsible for the blue, green, and red emissions [10,12]. Blue emission is caused by the electron transition from the shallow donor level (ionised oxygen vacancies) to the top of the valence band, which occurs at the luminescence peaks of 450 and 483 nm [13,14]. Peak at 478 nm for CuO:Mn(0.2) gives the band gap transition which was well matched with the UV-Vis analysis. The luminescence peak at 483 nm (2.57 eV) for CuO:Mn(0.1), 479 nm (2.59 eV) for CuO:Mn(0.3) and 592 nm (2.09 eV) for CuO:Mn(0.3):Sr corresponds to NBE. The green (525nm),yellow-orange (600nm) emissions in CuO:Mn and red (746 nm) emission in CuO:Mn(0.3):Sr arise from recombination of electrons in the V'_0 (singly ionized oxygen vacancy) center with photoexcited holes (h^+) in the valence band. The Mn and Sr doping shift the conduction band and valence band levels in relation to the V'_0 level, leading to the efficient red luminescence upon irradiation of excitation radiation. For CuO, CuO:Mn and CuO:Mn(0.3):Sr nanoparticles, emission due to oxygen vacancy (especially the singly ionized oxygen vacancy, V'_0) is more intense than band edge and near band edge emissions. It's relevant that Sr co-doping reduces the intensity of CuO:Mn's NBE and emission in the higher wavelength areas. The Sr doping introduced more defects in the system. As a result, the NBE peak caused by actual exciton recombination has been steadily repressed by the increasing amount of defect center-induced (singly occupied oxygen vacancy) recombination. Mn and Co doped ZnO nanorods were discovered to have similar luminescence lowering effects [15]. It might be because the doped cations offer strong recombination routes, which reduces the intensity of the emission. When it comes to the system's optical properties, it has been noticed that Sr doping introduces more and more defects or disorder, which has significantly altered the system's optical properties.

All the samples show a band gap or near band gap emission which was a conformation to the band gap obtained from UV-Vis analysis. The defect emission from CuO nanoparticles in blue region got shifted to yellow-orange region with Mn doping which is further shifted to red region with Sr co-doping. This shows the influence of doping over defect level emission.

4. Conclusion

The chemical co-precipitation method was successful in producing CuO, Manganese-doped CuO nanoparticles. Through the use of a solid state process, strontium is co-doped in CuO:Mn. The formation of single phase CuO nanoparticles is confirmed by the XRD spectrum. The sample's peak locations show that CuO has a monoclinic structure. The monoclinic structure's lattice parameters were determined to be a = 4.685 Å, b = 3.425 Å, c = 5.130 Å, and β= 99.549^0. The size of the crystallite increases slightly following Mn doping because the ionic size of Mn^{2+} is bigger than that of Cu^{2+}. With the addition of strontium co-doping and an increase in manganese concentration, a modest rise in particle size was seen. FESEM was used for the morphological investigation, which revealed that doping changed the sample morphology. The elemental composition of the synthesised nanoparticles is confirmed by EDS data. The band gap of CuO narrows with Mn doping, according to optical studies. Sr co-doping into CuO:Mn(0.3) lowers the bandgap energy as well. The visible region of the PL spectra displayed strong blue, yellow-orange, and red emission peaks, which may be related to the

levels of surface defect brought on by impurities. With doping and co-doping, the visible emission intensity increases. When Sr was co-doped with CuO:Mn (0.3) samples, a quenching of PL emission intensity was seen. It could be because more defects have been introduced into the system as a result of Sr doping, and the doped cations offer competitive paths for recombination. The impact of Sr on CuO paves the way for additional research. In conclusion, the optical characteristics of the CuO nanoparticles are enhanced by the manganese and strontium co-doping.

References

1. Prabakaran S, Nisha K D, Harish S, Archana J, Navaneethan M, Ponnusamy S, Muthamizhchelvan C, Ikeda H, and Hayakawa Y. Synergistic effect of SnO2 and ZnO in enhancing the electrical and optical properties of Anatase TiO2. *Applied surface science*. **498**, no. 1 (2019) 143702.

2. Rafea M A, and Roushdy N. Determination of the optical band gap for amorphous and nanocrystalline copper oxide thin films prepared by SILAR technique. *Journal of Physics D: Applied Physics*. **42**(1) (2008) 015413.

3. Ponnar M, Thangamani C, Monisha P, Gomathi S S and Pushpanathan K. Influence of Ce doping on CuO nanoparticles synthesized by microwave irradiation method. *Applied Surface Science*. **449** (2018) 132-143.

4. Ahmed A, Ali T, Naseem Siddique M, Ahmad A and Tripathi P. Enhanced room temperature ferromagnetism in Ni doped SnO2 nanoparticles: A comprehensive study. *Journal of Applied Physics*. **122(8)** (2017) 083906.

5. Das S, Girija K G, Debnath A K and Vatsa R K. Enhanced NO2 and SO2 sensor response under ambient conditions by polyol synthesized Ni doped SnO2 nanoparticles. *Journal of Alloys and Compounds*. **854** (2021) 157276

6. Wesselinowa J M. Magnetic properties of doped and undoped CuO nanoparticles taking into account spin–phonon interactions. *Physics Letters A*. **375(11)** (2011) 1417-1420.

7. Schmid C, Nanoparticles, 1st edn. Wiley-VCH VerlagGmbH & Co, Weinheim (2004).

8. Chukwuocha E O, Onyeaju M C and Harry T S T. Theoretical Studies on the Effect of Confinement on Quantum Dots Using the Brus Equation. *World Journal of Condensed Matter Physics*. **2** (2012) 96-100.

9. Zhao X, Peng W, Zaoxue Y, and Naifei R. Room temperature photoluminescence properties of CuO nanowire arrays. *Optical Materials*. **42** (2015) 544-547.

10. Eliseev A A, Alexey V L, Alexey A V, Lyudvig I H, Alexandr I Z, and Yury D T. Complexes of Cu (II) with polyvinyl alcohol as precursors for the preparation of CuO/SiO2 nanocomposites. *Materials Research Innovations*. **3(5)** (2000) 308-312.

11. Xu J F, Ji W, Shen Z X, Tang S H, Ye X R, Jia D Z, and Xin X Q. Preparation and characterization of CuO nanocrystals. *Journal of Solid-State Chemistry*. **147(2)** (1999) 516-519.

12. Borgohain K, Jung B S, Rama Rao M V, Thoudinja S and Shailaja M. Quantum size effects in CuO nanoparticles. *Physical Review B*. **61(16)** (2000) 11093.

13. Xue Z Y, Zhang D H, Wang Q P and Wang J H. The blue photoluminescence emitted from ZnO films deposited on glass substrate by rf magnetron sputtering. *Applied surface science*. **195(1-4)** (2002) 126-129.

14. Roy V A L, Djurisic A B, Liu H, Zhang XX, Leung YH, Xie M H, Gao J, Lui H F and Surya C. Magnetic properties of Mn doped ZnO tetrapod structures. *Applied physics letters*. **84** (2004) 756–758.

15. Panigrahy B, Aslam M, and Bahadur D. Aqueous synthesis of Mn-and Co-doped ZnO nanorods. *The Journal of Physical Chemistry C*. **114(27)** (2010) 11758-11763.